

Simulation of Three-Dimensional Flow of Light Non-Aqueous Phase Liquids in an Unsaturated-Saturated Zone

Rafa H. Al-Suhaili¹ and Ayad A. H. Faisal²

1 The Senior Prof. of the Civil Engineering Dept., University of Baghdad, Iraq.

A Visiting Prof. to the City College, City University of New York, USA.

2 Assistant Prof., Env. Engineering Dept., College of Engineering, University of Baghdad, Baghdad, Iraq.

Abstract: - A three-dimensional finite difference model that describes the infiltration and redistribution of light non-aqueous phase liquid (LNAPL) for the state of the three fluid phases; water, oil and air in the unsaturated-saturated zone of the soil is developed. The present model tracks the percentage of oil saturation as well as the lateral and vertical position of the oil plume in the subsurface, resulting from oil spillage, at the specified times with different types of boundary conditions. The flow equations are cast in terms of the wetting and non-wetting fluid pressure heads, respectively. The present model is validated through comparison to a laboratory three-dimensional experiment involving the infiltration and redistribution of kerosene into a sand bed. Results proved that the oil saturation in the upper part of the soil section declined towards a constant value, while the water saturation during the redistribution stage gradually increases in a linear form.

Keywords: - LNAPL; Oil migration; Sand bed; Numerical modeling; Electrical resistance; Unsaturated zone.

I. INTRODUCTION

Non-aqueous phase liquids (NAPLs) have been discovered at numerous hazardous waste sites. As compounds such as hydrocarbon fuels, organic solvents, and other immiscible organic liquids migrate through unsaturated-saturated zone they will pollute large extents of soil and groundwater (Fig.1). These organic fluids form a serious threat to groundwater resources, for example one liter of oil can significantly affect the quality of 100000 liters of water and consequently this water cannot be used (Marsman, 2002).

A number of multiphase flow models in the contaminant hydrology literature have been presented. Faust (1985) presented an isothermal two-dimensional finite difference simulator which describes the simultaneous flow of water and NAPL under saturated and unsaturated conditions. Faust et al. (1989) developed a model that can be used to simulate a three-dimensional two-phase transient flow system based on a finite difference formulation. The governing equations were cast in terms of non-wetting fluid (NAPL) pressure and water saturation. Similarly, Parker et al. and Kuppusamy et al. as cited in Suk (2003) developed a two-dimensional multiphase flow simulator involving three immiscible fluids: namely, air, water and NAPL with the assumption of a constant air phase pressure. Kaluarachchi and Parker (1989) applied a two-dimensional finite element model named MOFA-2D for three phases, multi-component, isothermal flow and transport by allowing for inter-phase mass exchange but assuming gas phase pressure gradients are negligible. Pantazidou and Sitar (1993) presented experimental and analytical investigations of the movement of lighter than water organic liquids in the vadose zone. The experiments consisted of physical model tests simulating NAPL spills in unsaturated, two-dimensional domains above the water table. Darnault et al. (2001) developed a method by which fluid content can be measured rapidly in three-phase systems. This method uses the hue and intensity of light transmitted through a two-dimensional slab chamber to measure fluid contents. Kim and Corapcioglu (2003) developed a vertically averaged two-dimensional model to describe a real spreading and migration of LNAPL introduced into the subsurface by spills or leaks from underground storage tanks. This model is represented the transport of LNAPL lens in X-Y plane which is formulated on water table after spill.

Kechavarzi et al. (2005) presented a quantitative two-dimensional laboratory experiment to investigate the immiscible flow of a LNAPL in an unsaturated zone under homogenous soil conditions. An image analysis technique was used to determine the two-dimensional saturation distribution of LNAPL, water and air during LNAPL infiltration and redistribution. Ojuri[10] introduced an experimental and numerical investigation with the aim of characterizing the source, extent, transport and fate of petroleum hydrocarbon contamination in a 3D sand tank model and at the case study field sites, appraising the implication of the results for evaluating remediation endpoints. Singh (2010) presented an analytical solution of 1D solute transport equation to predict the contaminant concentration distribution along and against transient groundwater flow in finite homogenous aquifer. Kamaruddin et al. (2011) introduced the methodology for two-dimensional light non-aqueous phase liquid experiments with the application of light reflection and light transmission methods associated with image analysis methods including the process of visualizing simulation results that has improved on lengthy and tedious conventional methods. Sulaymon and Gzar(2011) studied the dissolution and transport process of benzene as a LNAPL in saturated porous media. This process was studied under unidirectional flow at different water velocities ranging from 0.90 to 3.60 cm/hr in a three-dimensional saturated sand tank with dimensions of 100×40×35 cm.

The significance of the present study is (a) characterization of Kerbala's sand for unsaturated flow of kerosene depended on a physical model that simulates an oil spill into a sand bed in a three-phase three-dimensional system, and (b) demonstrating that the governing equations and their solution procedure is representative of flow behavior of the kerosene in the unsaturated-saturated zone.

II. THEORY AND NUMERICAL FORMULATION

In the present analysis, the pressure gradient in the gas phase is assumed to be negligible so that gas pressure remains effectively constant at atmospheric pressure (Faust et al., 1989). Assuming also an incompressible porous medium and constant fluid properties, the flow equation for water (w) and organic liquid phase (o) may be written in summation convection for a three-dimensional Cartesian domain as (Bear, 1972):-

$$\frac{\partial}{\partial x} \left[K_w \frac{\partial h_w}{\partial x} \right] + \frac{\partial}{\partial y} \left[K_w \frac{\partial h_w}{\partial y} \right] + \frac{\partial}{\partial z} \left[K_w \left(\frac{\partial h_w}{\partial z} + 1 \right) \right] = C_w \frac{\partial h_w}{\partial t} \quad (1)$$

where x, y and z are the Cartesian spatial coordinates; K_w and K_o are conductivity tensors for water and oil respectively; h_w and h_o are the water height-equivalent pressure heads of water and oil respectively; ρ_{ro} is the ratio of oil to water density; t is the time. Phase conductivities are assumed to be described by:

$$K_w = K_{ws} K_{rw}, \quad K_o = \frac{K_{ws} K_{ro}}{\mu_{ro}} \quad (3)$$

where K_{rw} and K_{ro} are relative permeabilities of water and oil respectively, μ_{ro} is the oil and water viscosity ratio, and K_{ws} is the saturated conductivity tensor for water. The terms C_w and C_o are the specific fluid capacity defined as follows:-

$$C_w = \phi \frac{\partial S_w}{\partial h_w}, \quad C_o = \phi \frac{\partial S_o}{\partial h_o} \quad (4)$$

where ϕ is the porosity of the medium; S_w and S_o are the saturation of water and oil respectively.

Constitutive relationships used here to describe three-phase fluid relative permeabilities and saturations as functions of fluid heads described by Parker et al.(1987) which is based on Van Genuchten's (1980) model are:-

$$S_e = \frac{S_w - S_r}{1 - S_r}, \quad S_{te} = \frac{S_t - S_r}{1 - S_r} \quad (5)$$

$$S_e = [1 + (\alpha h_{aw})^n]^{-m} h_o \leq h_o^{cr} \quad (7)$$

$$h_o^{cr} = \frac{\beta_{ow} h_w}{(\beta_{ao} + \beta_{ow})} \quad (8)$$

$$S_{te} = [1 + (\alpha \beta_{ao} h_{ao})^n]^{-m} \quad (9)$$

where h_{ow} oil-water capillary pressure head ($=h_o-h_w$); h_{ao} air-oil capillary pressure head ($=h_a-h_o$); h_a the water height-equivalent pressure head of air; S_e effective water saturation; S_r residual water saturation; S_t total liquid saturation; S_{te} effective total liquid saturation and oil saturation $S_o=S_r-S_w$. Here α , n and $m(=1-1/n)$ are Van Genuchten's soil parameters, β_{ao} & β_{ow} are fluid-dependent scaling coefficients. The values of S_r , α , n , ϕ , β_{ao} , β_{ow} , μ_{ro} and ρ_{ro} for kerosene-water system in the sand adopted in the present study were 7%, 0.048 cm⁻¹, 2.7, 0.415, 2.75, 1.57, 1.512 and 0.8 respectively (Faisal, 2006).

The solution techniques used here consist of a finite-difference approximation, the Newton-Raphson numerical approach with a Taylor series expansion to treat nonlinearities. These techniques result in the general form of the matrix system:-

$$A^k \delta^{k+1} = -r^k \quad (12)$$

where A is the coefficient matrix for the linearized system and r^k is the residual in node (i,j,l) at iteration k . For each node, there is one linear equation in seven variables $\delta_{fi-1,j,l}^{k+1}$, $\delta_{fi,j-1,l}^{k+1}$, $\delta_{fi,j,l-1}^{k+1}$, $\delta_{fi,j,l}^{k+1}$, $\delta_{fi+1,j,l}^{k+1}$, $\delta_{fi,j+1,l}^{k+1}$ & $\delta_{fi,j,l+1}^{k+1}$. The collection of equations for each solution node leads to a global diagonal coefficient matrix of bandwidth ($=2 \times$ number of columns of discrete flow domain \times number of blocks of discrete flow domain $+1$). This matrix is solved for δ and then the algorithm enters the next iteration with new values of h_f evaluated as follows:-

$$h_{fi,j,l}^{k+1} = h_{fi,j,l}^k + \omega_f^{k+1} \delta_{fi,j,l}^{k+1} \quad (13)$$

where ω_f^{k+1} is a damping parameter as mentioned by Cooley (1983). The convergence criterion used for a given phase is as follows:-

$$\frac{\max. |\delta_{fi,j,l}^{k+1}|}{\max. |h_{fi,j,l}^k + \delta_{fi,j,l}^{k+1}|} \leq \varepsilon \quad (14)$$

where ε is the convergence tolerance. A typical convergence criterion for pressure head is 0.001 or less.

Two types of boundary conditions are considered. Firstly, Dirichlet or a fixed head boundary condition and secondly, Neumann or a specified flux condition. The present model ignores the transport of dissolved and vapour plume of NAPL. A computer program written in DIGITAL VISUAL FORTRAN (version 5) was developed to implement the model described above.

III. MODEL VALIDATION

In order to illustrate that the governing equations and the constitutive relationships upon which the numerical model is based correctly represent the intended real-life processes, the numerical model results are compared with results obtained from a three-dimensional sand bed experiment. The laboratory experiment involves a kerosene spill simulated in a three-dimensional tank 70 cm long, 45 cm high, and 20 cm wide. In all experiments, a total of 5000 cm³ of kerosene was used; this was equal to approximately 30% of the pore space above the water table. Kerosene was added as needed to maintain the height of the free liquid always at equivalent water pressure head equal to 4 cm above the top of the sand, until all 5000 cm³ of kerosene was used. The rate at which kerosene was added to maintain the level of 4 cm was dictated by the rate at which kerosene disappeared into the sand. The frame of the tank was made of steel to prevent bending of sides. All sides (front, back, lower and lateral boundaries) were made of 6 mm thick of glass which were transparent to allow for visual observations. The back side of the tank was supplied with a number of openings. Through these openings a pair of probes was inserted, which were connected to a resistance meter. These probes were located in a certain locations in the sand bed (Fig.2). The readings of the resistance meter were used to indicate the degree of water saturation. Two vertical partitions with lower openings that were 10 cm high and 20 cm wide, and covered with steel mesh formulate the lateral boundaries of the sand-filled middle compartment, their dimensions were (60×45×20) cm. The purpose of the two outer compartments was to provide constant head reservoirs for controlling the position of the water table within the sand deposited in the middle compartment. Each outer compartment was 5 cm long, 10 cm high, and 20 cm wide. The tank was placed in a room which was kept at 20°C. The tank was filled with 40 cm of Kerbala's sand which was used as the porous medium. The sand had a particle size distribution ranging from 50 μ m to 1mm (Fig.3) with an effective grain size, d_{10} , of 180 μ m, a median grain size, d_{50} , of 370 μ m and a uniformity coefficient, $C_u = d_{60}/d_{10}$, of 2.2. The permeability of the sand, measured with a constant head permeability test, was 115 cm/hr. Kerosene dyed with Sudan III was used as the infiltrating LNAPL in the experiments.

The degree of water saturation was measured at certain locations through a certain section through-out the sand bed by using resistivity probes connected to a resistance meter. These measurements were based on

electrical resistance between the two probes (electrodes). Electrical resistance measurements were converted to water saturation values with the aid of calibration curve determined experimentally for Kerbala's sand and the pore fluid (Fig.4), a 0.01N sodium chloride solution in deionized water used in the present study as recommended by Pantazidou and Sitar (1993). The NaCl solution was preferred to pure water because it delays dissolution of salts from the sand into the pore fluid and therefore provides a fluid of virtually constant electrical properties for which a single calibration curve can be used. On the other hand, Firoozabadi and Ramey in 1988 showed that salts affect the surface properties at high concentrations as cited by Pantazidou and Sitar (1993), the sodium chloride concentration was chosen to be low in order to minimize change of the interfacial tension between water and the NAPL. Measurement of water pressure was achieved by using a tensiometer. Water saturation measurements were converted to water pressure values with the aid of a calibration curve determined experimentally for Kerbala's sand (Fig.5). As water saturations were measured with the time at the locations illustrated in Fig.2, the corresponding water pressure can be calculated by using the water pressure-saturation calibration curve shown in Fig.5. By using these values and the constitutive relationships adopted for kerosene-water system in Sec.2, the corresponding oil pressure and oil saturation can be calculated.

IV. RESULTS AND DISCUSSION

The present study provides an example of a fully three-dimensional flow field in laboratory scale in which kerosene, air, and water are present. This problem is reflected the ability of the present model to solve any three-dimensional case subjected to a given geometry, boundary conditions, and initial conditions. The geometry of the flow domain, as described in the Sec.3, is represented by middle compartment of the tank which is the location of the sand bed. This bed has the dimensions of 60 cm long (in x-direction), 40 cm high (in z-direction) and 20 cm wide (in y-direction). Kerosene was introduced into the sand bed from cubic container. This container has the dimensions of 10 cm long, 6 cm high and 5 cm wide. The centerlines of this container coincide with centerlines of the top view of the tank.

The properties of the soil and kerosene used in the present simulation are mentioned in Sec.2. Oil was allowed to infiltrate from the container under a water equivalent oil pressure head of 4 cm to simulate an oil spill. For the water phase, constant head boundary conditions were imposed for the saturated zone. Zero-flux boundaries were used on all other boundaries. For the oil phase, all boundaries except the source were zero flux. For all cases a total of 5000 cm³ of kerosene was permitted to infiltrate. Redistribution was allowed up to a total simulation time of 24 hours.

The three-dimensional finite-difference grid extends 30 cm from the center of the source in a positive x-direction, 40 cm vertically downward in the z-direction and 10 cm from the center of the source in a positive y-direction, discretizing the field into 315 blocks. The present model assumes a symmetrical grid, therefore, negative x- and y- values are implied and presumed equivalent to the simulated positive x- and y- values respectively. Variable time step sizes (ranged from 0.0001 to 0.1 hrs) were used in solving the present problem. The present problem was simulated in two steps. The first step established a steady state flow field based on the boundary conditions which was used as initial condition for the transient simulation. The second step, the transient simulation, consisted of two periods. During the first period (21.2 min as calculated from the present model and 23 min as calculated from the present experimental work), leakage of kerosene into the sand bed is equal to 235.78 cm³/min. Because the present model has the advantage of symmetry in the x and y directions to reduce by quarter the number of blocks, the modeled source rate is 58.945cm³/min. As illustrated in Fig.6, there is a good agreement between the calculated and measured cumulative oil infiltration. During the second period, there is no leakage of kerosene into the sand bed, but the accumulated kerosene during the first period was allowed to redistribute for a total simulation time equal to 24.0 hours.

The present experimental results of effective water saturation, capillary pressure and oil saturation in locations 1, 2 and 3 are compared with the corresponding computed values as shown in Figs.7, 8 and 9. The following remarks may be made on these figures: - (1) it is seen that there is a good agreement between computed values of effective water saturation and capillary pressure with corresponding experimental values. While the computed values of oil saturation are slightly larger than the experimental values. It seems that this departure of the experimental results from the theoretical model is due to the effect of dissolution and volatilization which are neglected in the present theoretical model. The present model does not consider dissolution or volatilization and, therefore, provides a conservative estimate of the extent of NAPL migration. Kerosene that migrates to a position at or near the ground surface will likely vaporize and enter the atmosphere. This volatilization will effectively reduce saturation levels. Also, relatively soluble chemicals would sustain a loss of mass as the NAPL dissolves and disperses into the surrounding groundwater. (2) As the time is increased beyond the infiltration stage the water saturation increases, the oil saturation decreases and both the theoretical and experimental water and oil saturation versus time relation are, approximately, linear.

According to Fig.10, the maximum kerosene saturation (0.986 at t = 21.2 min) occurred below the line source during the kerosene infiltration. During redistribution, this value at the same position decreased to (0.411 at 24

hours). Also, the reduction in kerosene saturation and the gradual increase in water saturation as the front approached the water table, resulted in a reduction in the kerosene relative permeability and therefore caused a decrease in the front velocity.

V. CONCLUSIONS

(1) The numerical solution based on the potential form of the governing equations using a finite-difference approximation, the Newton-Raphson numerical approach with a Taylor series expansion was shown to be efficient in solving three-dimensional water and LNAPL flow through the unsaturated-saturated zone in a three fluid phase system.

(2) The calculated oil saturations for three-dimensional simulation from the present model were slightly greater than the corresponding experimental values. This departure is due to neglecting the volatilization and dissolution mechanisms associated with the LNAPL transport through the unsaturated-saturated zone of the soil. In real spillage, the part of LNAPL will vaporize into the air phase and, on the other hand, another part will dissolve into the water phase. Consequently, for this reason, the actual remaining of LNAPL will less than the calculated values.

(3) As the time is increased beyond the infiltration stage the water saturation increases, the oil saturation decreases and both the theoretical and experimental water and oil saturation versus time relation are, approximately, linear. However, saturation or capillary pressure as a function of time at the chosen points show a rapid early rise followed by an essential uniform plateau.

(4) The reduction in kerosene saturation and the gradual increase in water saturation as the front approached the water table, resulted in a reduction in the kerosene relative permeability and therefore caused a decrease in the front velocity.

REFERENCES

- [1] Bear, J., "Dynamics of fluids in porous media". Elsevier, New York, 1972.
- [2] Cooley, R.L., "Some new procedures for numerical solution of variably saturated flow problems". Water Resources Research, 19(5), 1271-1285, 1983.
- [3] Darnault, C.J., D. A. Dicarolo, T. W. Bauters, A. R. Jacobson, J. A. Throop, C. D. Montemagno, J. Y. Parlange, and T. S. Steenhuis, "Measurement of fluid contents by light transmission in transient three-phase oil-water-air systems in sands". Water Resources Research, 37(7), 1859-1868, 2001.
- [4] Faisal, A.A.H., "Numerical modeling of light non-aqueous phase liquid spill transport in an unsaturated-saturated zone of the soil". Ph.D. Thesis, Baghdad University, 2006.
- [5] Faust, C., J. Guswa, and J. Mercer, "Simulation of three-dimensional flow of immiscible fluids within and below unsaturated zone". Water Resources Research, 25(12), 2449-2464, 1989.
- [6] Faust, C.R., "Transport of immiscible fluids, within and below the unsaturated zone : A numerical model". Water Resources Research, 21(4), 587-596, 1985.
- [7] Kaluarachchi, J.J., and J.C. Parker, "An efficient finite element method for modeling multiphase flow". Water Resources Research, 25, 43-54, 1989.
- [8] Kamaruddin, A., N.A. Sulaiman, A. Rahman, M.P. Zakaria, M. Mustaffar, and R. Saari, "A review of laboratory and numerical simulations of hydrocarbons migration in subsurface environments". Journal of Environmental Science and Technology, 4(3), 191-214, 2011.
- [9] Kechavarzi, C., K. Soga, and T. H. Illangasekare, "Two-dimensional laboratory simulation of LNAPL infiltration and redistribution in the vadose zone". J. of Contaminant Hydrology, 76, 211-233, 2005.
- [10] Kim, J., and M.Y. Corapcioglu, "Modeling dissolution and volatilization of LNAPL sources migrating on the groundwater table". J. of Contaminant Hydrology, 65, 137-158, 2003.
- [11] Marsman, A., "The influence of water percolation on flow of light non-aqueous phase liquid in soil". Ph.D. Thesis, Wageningen University, Wageningen, library.wur.nl/wda/dissertations/dis3306.pdf, 2002.
- [12] Ojuri, "Plume behaviour for petroleum hydrocarbon in a tropical sand tank: laboratory experiments and scenario-specific modeling". European Journal of Scientific Research, ISSN 1450-216X, 39 (4), 523-541, 2010.
- [13] Pantazidou, M., and N. Sitar, "Emplacement of non-aqueous liquids in the vadose zone". Water Resources Research, 22(1), 25-33, 1993.
- [14] Parker, J. C., R. J. Lenhard, and T. Kuppasamy, "A parametric model for constitutive properties governing multiphase flow in porous media". Water Resources Research, 23(4), 618-624, 1987.
- [15] Singh, M.K., "Analytical solution for contaminant transport along and against time dependent source concentration in homogeneous finite aquifers". Adv. Theor. Appl. Mech., 3(3), 99-119, 2010.
- [16] Suk, H., "Development of 2- and 3-D simulator for three phase flow with general initial and boundary conditions on the fractional flow approach". Ph.D. Thesis, Pennsylvania State University, 2003.

- [17] Sulaymon, A., and H.A. Gzar, "Experimental investigation and numerical modeling of light non-aqueous phase liquid dissolution and transport in a saturated zone of the soil". Journal of Hazardous Materials, 186, 1601–1614, 2011.
- [18] Van Genuchten, M., "A closed-form equation for predicting the hydraulic conductivity of unsaturated soils". Soil Sci. Soc. Am. J., 44, 892-898, 1980.

SYMBOLS

The following symbols are used in this paper:

A = coefficient matrix;	K_{rw} = relative permeability of water;
C_o = specific oil capacity;	k = iteration index;
C_w = specific water capacity;	n, m Van Genuchten's soil parameters;
C_u = uniformity coefficient;	r = the residual due to approximation;
d_{10} = effective grain size (L);	S_e = effective of water saturation;
d_{50} = median grain size (L);	S_o = oil saturation;
h_a = air pressure head (L);	S_t = total liquid saturation;
h_{ao} = air-oil capillary pressure head (L);	S_{te} = effective total liquid saturation;
h_{aw} = air-water capillary pressure head (L);	S_r = residual water saturation;
h_f = fluid pressure head (L);	t = time coordinate (T);
h_o = oil pressure head (L);	x, y, z = cartesian coordinates;
h_o^{cr} = critical oil pressure head (L);	α = Van Genuchten's soil parameter (L);
h_{ow} = oil-water capillary pressure head (L);	β_{ij} = fluid-dependent scaling coefficient;
h_w = water pressure head (L);	δ = the difference between the approximation and exact solution (L);
i, j, l = grid identification in x, y, z directions respectively;	ε = convergence tolerance;
K_o = hydraulic conductivity of oil ($L T^{-1}$);	μ_{ro} = viscosity ratio between oil and water
K_w = hydraulic conductivity of water ($L T^{-1}$);	ρ_{ro} = ratio of oil to water density;
K_{ws} = saturated conductivity tensor for water ($L T^{-1}$);	ϕ = porosity of the medium;
K_{ro} = relative permeability of oil;	ω = damping parameter;

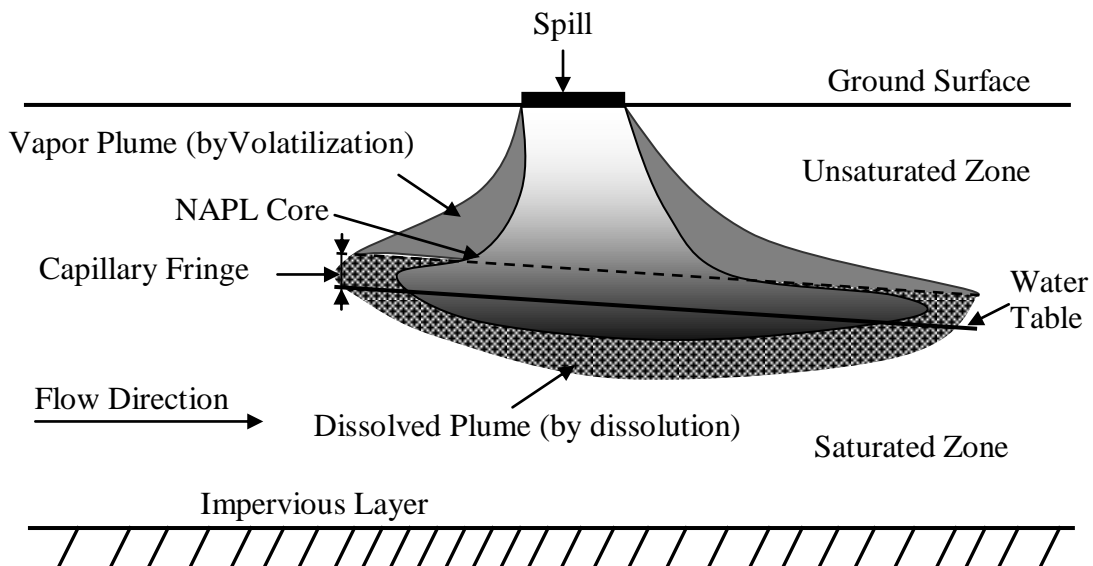


Fig. 1. Conceptualized representation of LNAPL migration and contamination of the subsurface (Faisal, 2006).

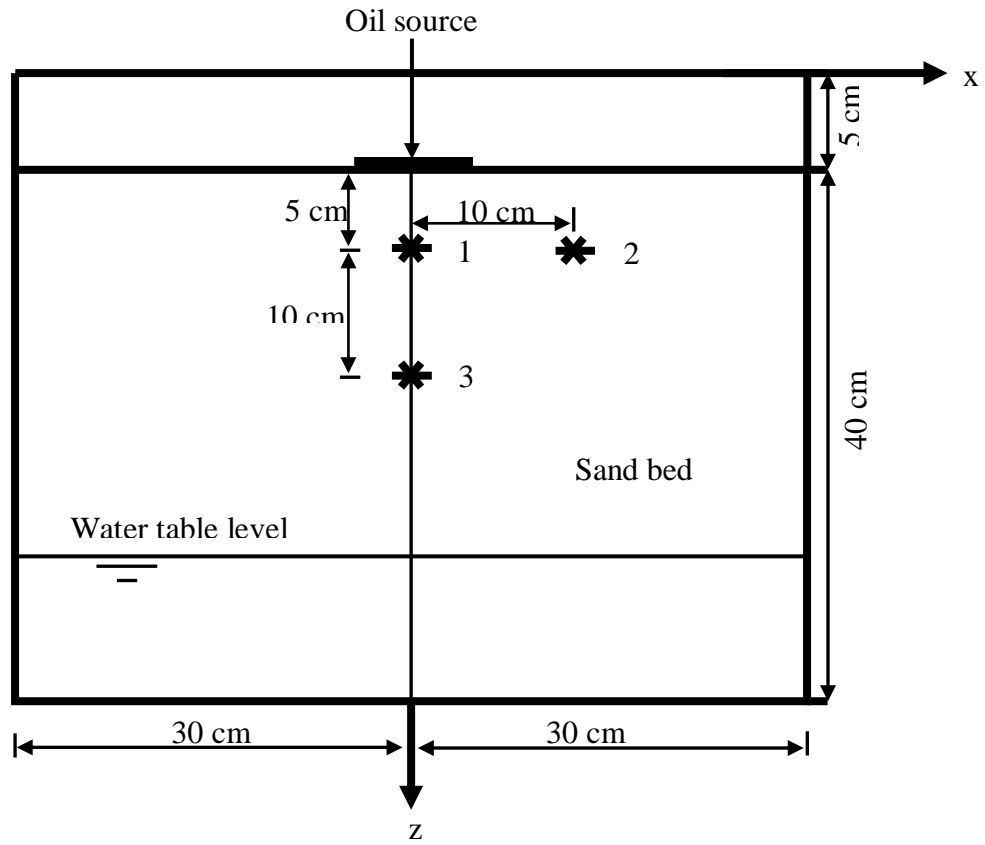


Fig. 2. Selected locations (1, 2 and 3) in the central section for measurement of phases variables during the present study.

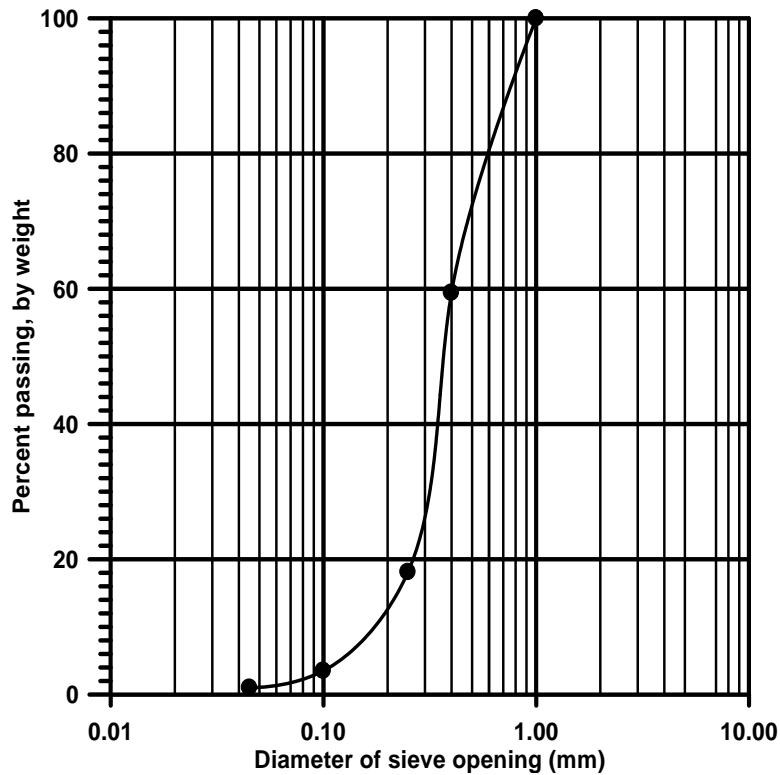


Fig. 3. Gradation curve for Kerbala's sand.

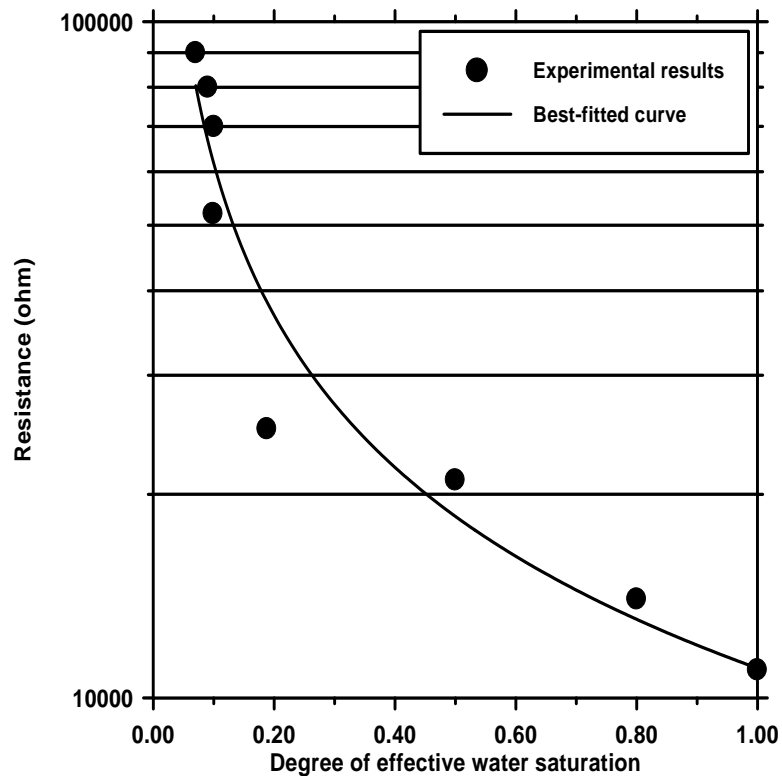


Fig. 4. Electrical resistance-water saturation curve for Kerbala's sand.

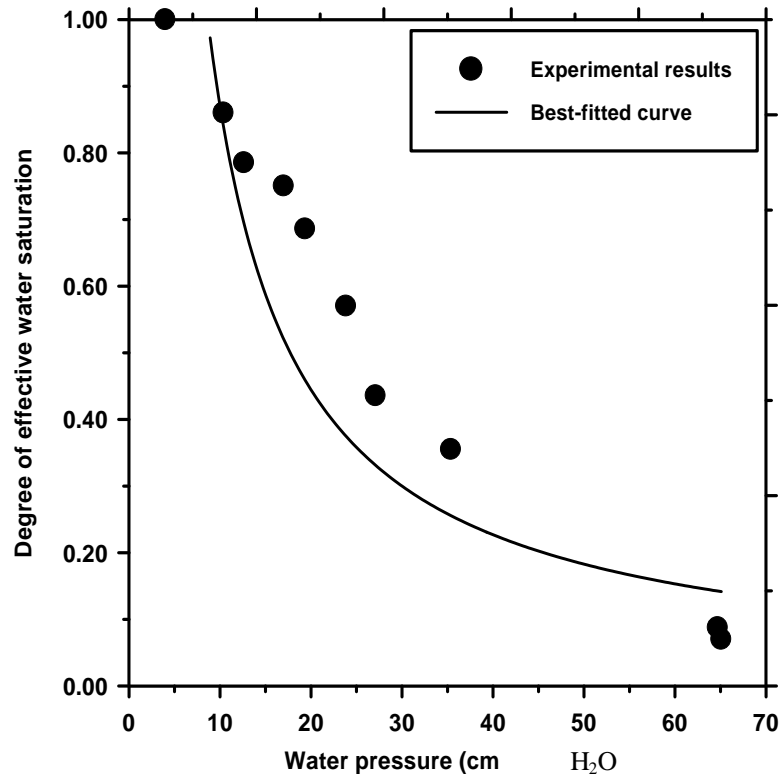


Fig. 5. Water pressure-water saturation curve for Kerbala's sand.

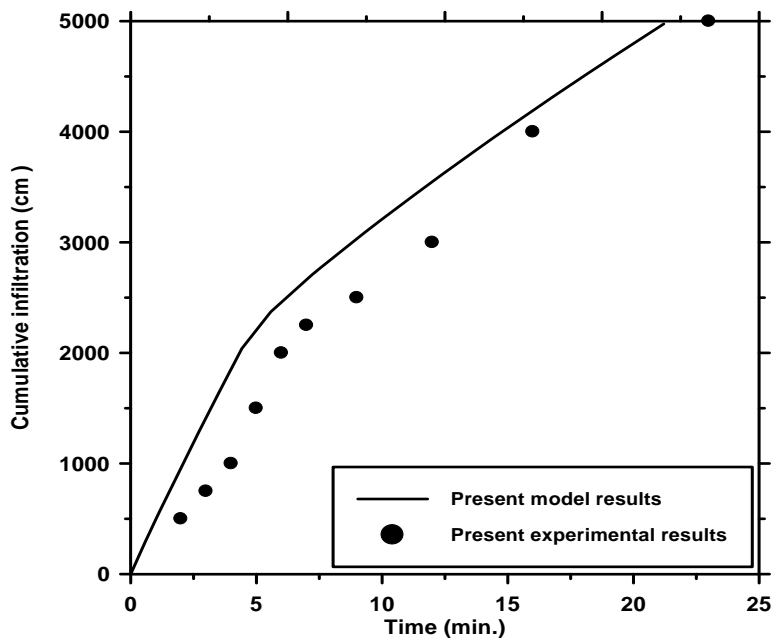
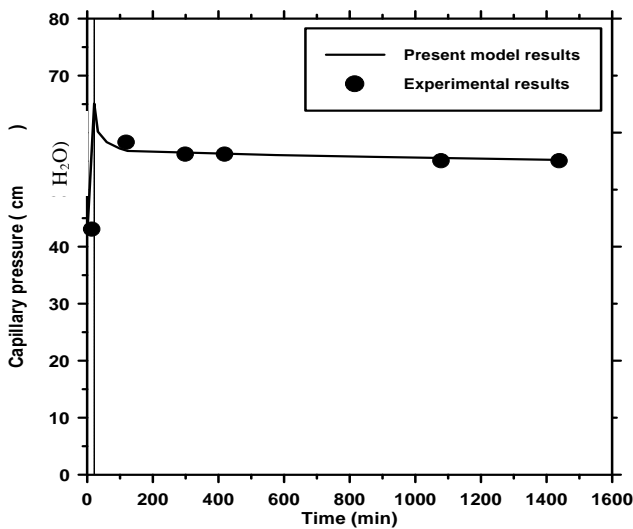
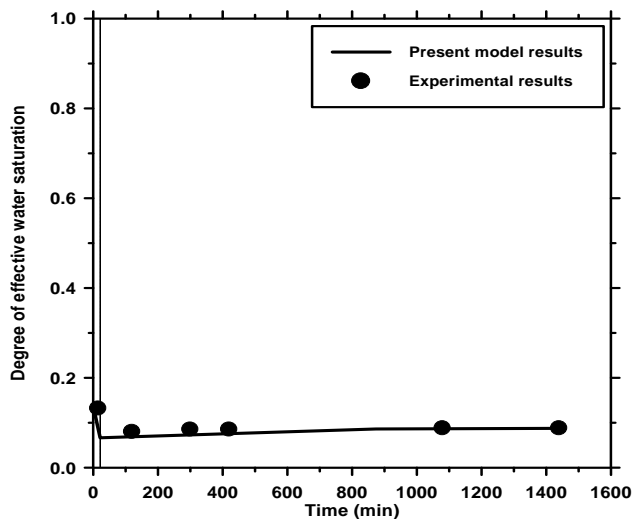


Fig. 6. Cumulative oil infiltration versus time for the three-dimensional simulation.



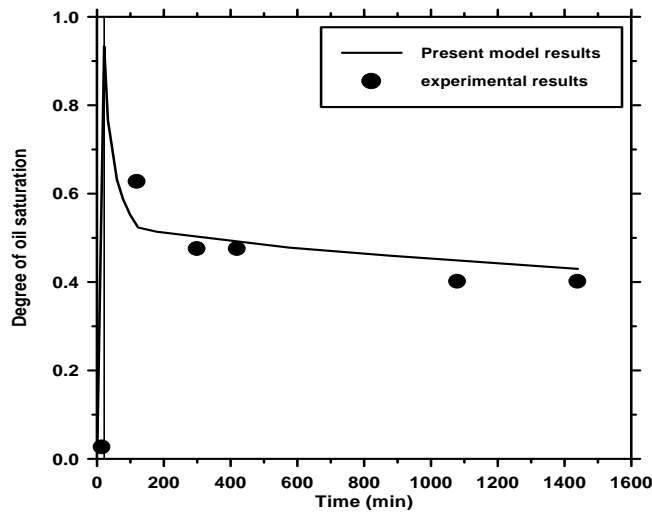
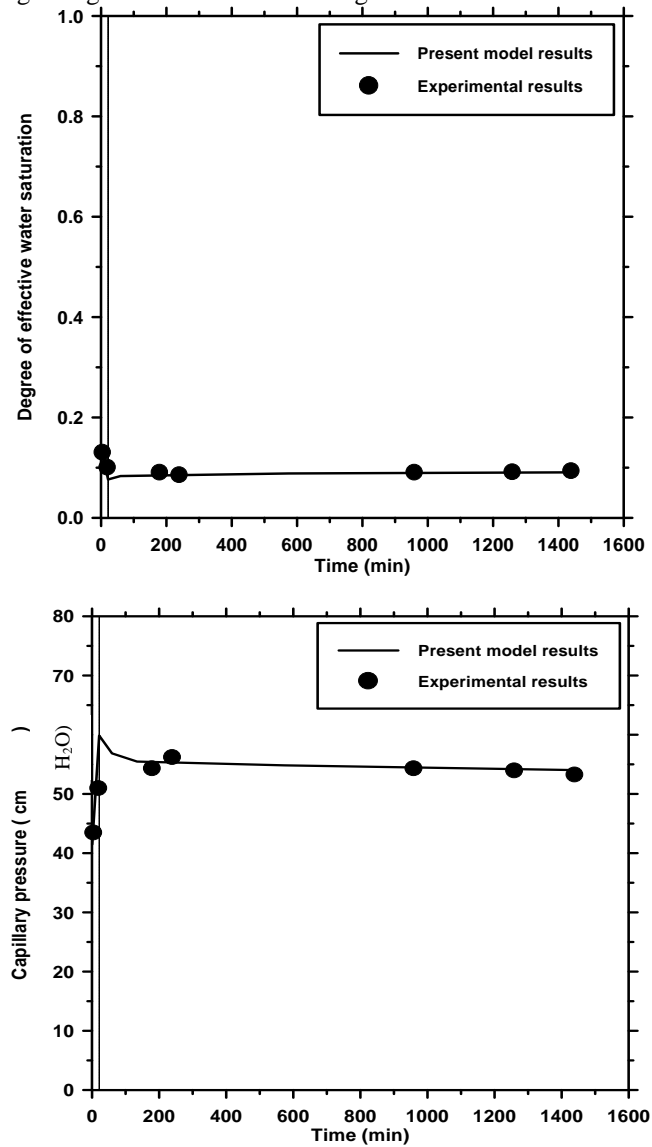


Fig. 7. Water saturation, capillary pressure and kerosene saturation changes with time during kerosene infiltration and redistribution registered at location 1 in the sand bed, dashed line marks the end of the infiltration stage and the beginning of the redistribution stage.



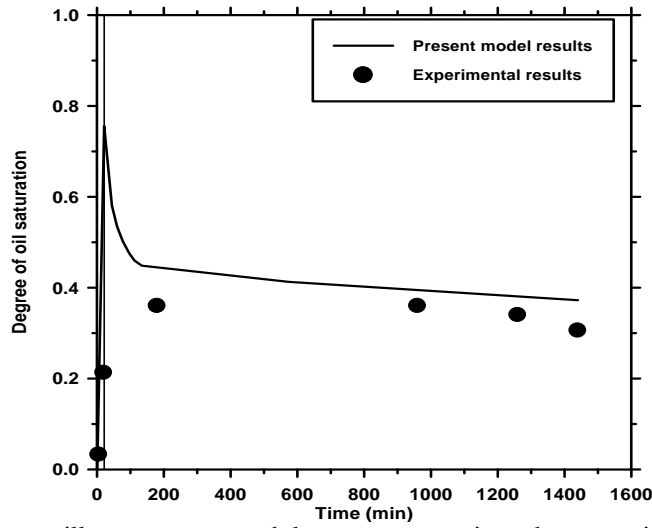
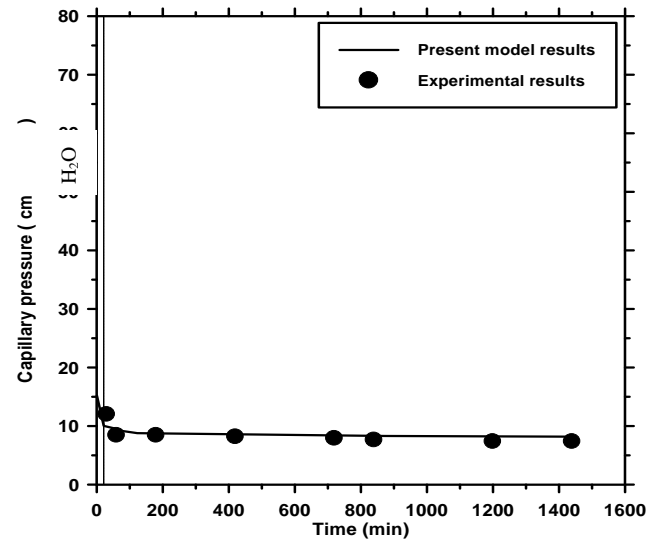
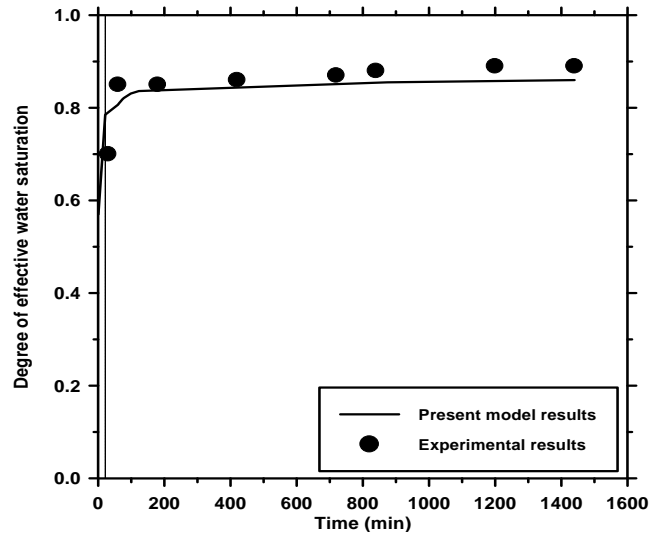


Fig. 8. Water saturation, capillary pressure and kerosene saturation changes with time during kerosene infiltration and redistribution registered at location 2 in the sand bed, dashed line marks the end of the infiltration stage and the beginning of the redistribution stage.



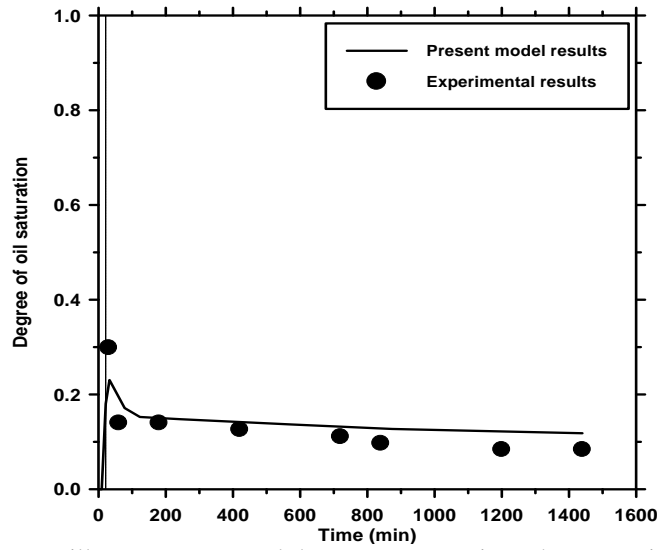


Fig. 9. Water saturation, capillary pressure and kerosene saturation changes with time during kerosene infiltration and redistribution registered at location 3 in the sand bed, dashed line marks the end of the infiltration stage and the beginning of the redistribution stage.

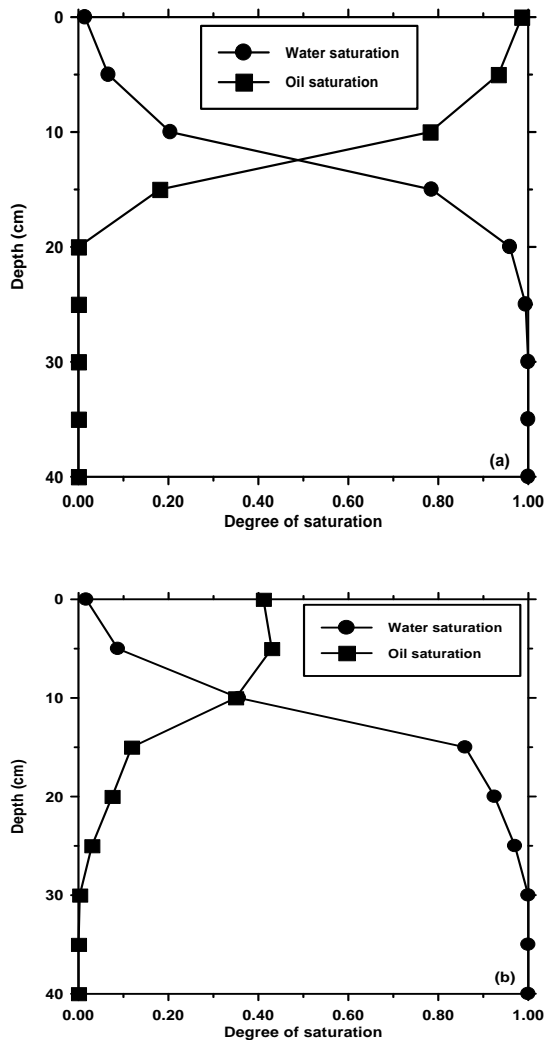


Fig. 10. Kerosene and water saturation profiles calculated on the center line of the tank after (a) 21.2 min and (b) 24 hours.